https://doi.org/10.15407/tpwj2019.09.02

EFFECT OF COOLING CYCLE OF WELDING ON STRUCTURE-PHASE COMPOSITION OF 15Kh2NMFA STEEL

O.V. MAKHNENKO, V.A. KOSTIN, V.V. ZHUKOV and **E.S. KOSTENEVICH**
E.O. Paton Electric Welding Institute of the NAS of Ukraine
11 Kazymyr Malevych Str., 03150, Kyiv, Ukraine. E-mail: office@paton.kiev.ua

In the recent years, mathematical methods are widely used for prediction of microstructure-phase composition of structural steels under thermal effect. Using mathematical modeling based on existing parametric regression equations there was carried out prediction of microstructure-phase transformations in HAZ metal of base material (steel 15Kh2NMFA) of WWER-1000 reactor vessel in arc cladding of protective anti-corrosion layer as well as performed comparative analysis of modeling results with obtained experimental data of dilatometric and metallographic analysis. The comparison of results ensures formation of bainite-martensite structure in HAZ metal of WWER-1000 reactor vessel, however a value of content of martensite in calculation and experimental determination is significantly different. For calculation determination of content of structural constituents it is necessary to use the experimental CCT diagrams of undercooled austenite decay for characteristic welding/cladding thermal cycles, which do not have long-term heating or holding at austenitizing temperature and cooling takes place with variable rate. CCT diagrams of undercooled austenite for typical cooling rates 3–5 °C/s and two maximum temperatures of thermal cycle, namely 1000 and 1350 °C were experimentally plotted for adequate evaluation of microstructure composition in HAZ metal of vessel steel 15Kh2NMFA in welding/cladding. Obtained results can be used in calculation determination of residual stresses in WWER-1000 reactor vessel for grounding the extension of safe operation life. 32 Ref., 7 Tables, 12 Figures.

Keywords: *WWER-1000 reactor vessel, steel 15Kh2NMFA, anti-corrosion cladding, microstructure transformations, mathematical modeling, dilatometry*

In Ukraine the most part of nuclear power units is referred to WWER-1000 type, reactor vessel (RV) of which is made of thick-wall forged shells of low-alloy high-strength steels of pearlite class of 15Kh2NMFA grade, welded by girth welds. To protect RV from corrosion the austenite material is built up on its inner surface. Currently, an important scientific-technical problem is extension of safe operational life of working RV. Its substantiation requires taking into account residual stresses appearing as a result of welding or cladding heating, and their redistribution in process of further heat treatment.

Technological parameters of process of anti-corrosion cladding can have significant effect on microstructure-phase composition in heat-affected zone (HAZ) of 15Kh2NMFA steel as well as distribution of residual stresses in WWER-1000 RV.

Analysis of open access references shows [1–7] that they do not have data relatively to microstructure-phase composition of reactor vessel steel after arc cladding as well as there is no its complete CCT diagram of undercooled austenite decay. Existing metallurgical CCT diagrams of reactor steels [8, 9], obtained for typical in performance of heat treatment long-term holdings at maximum temperature and low cooling rates, do not allow determining final microstructure-phase composition of metal in HAZ due to peculiarities of welding/cladding thermal cycle.

There are data [10] that there is formation of bainite-martensite microstructure in HAZ metal at cooling rate 3.3–28 °C/s in 800–500 °C temperature range for steel 15Kh2NMFA and critical cooling rate, above which completely martensite structure is formed in HAZ metal, makes 30 °C/s. The results, obtained in work [11], vice versa, show that typical welding cycle with metal cooling rate 3–6 °C/s can provoke formation of mainly martensite microstructure. In foreign atlases and collections of CCT diagrams there are no data for reactor vessel steel 15Kh2NMFA at heat treatment and welding of steels [12–14].

New data [15–17] on transformations in reactor vessel steels 15Kh2MFA-A and 15Kh2NMFA under conditions of different thermal cycles of cooling were presented in the recent time. Analysis of CCT diagrams of these steels shows presence of specific differences of temperatures of start and end of phase transformations, critical cooling rates and fractions of structural constituents. These differences, apparently, are related, on the one hand, with various composition of researched reactor vessel steels (absence of nickel in steel 15Kh2MFA-A), and on the other hand with difference of methods (devices), used for determina-

Table 1. Characteristics of conditions of CCT diagram plotting

Reference	Type of device	Dimensions of sample, mm	Austenitizing temperature, °C	Austenitizing time, min	Range of cooling rates, °C/s	Steel grade
[15]	BAHR DIL 805	10×4	1000	180	0.1–500	15Kh2MFA-A
[16]	Linseis L78 RITA	10×3	1000	20	0.01–50	15Kh2MFA-A
[17]	Linseis L75VD1600C	20×6	900	15	0.002–100	15Kh2NMFA

tion of temperature phase transformations, including, dimensions of samples and duration of holding in austenite area (Table 1).

In recent times, the mathematical models [18–21] got a large development for prediction of phase composition of structural steels at thermal effect. In this connection aim of the work lied in determination of possibility of application of mathematical modeling of kinetics of microstructure transformations in steel 15Kh2NMFA after arc cladding taking into account different technological parameters as well as performance of experimental verification (validation) of the calculation results using physical modeling of thermal-deformation state in welding/cladding.

Technological parameters of arc cladding of reactor vessel. In accordance to the requirements of reference documents [22] and following the documents of producing plant [23] automatic submerged-arc cladding with strip electrodes was used for cylinder part of reactor vessel and manual arc cladding with coated electrodes was used for surface of nozzle zone (inner surface of Du850 nozzle and their fillets) as well as other difficult-to-weld places of vessel. Table 2 provides cladding consumables.

According to [24–28] the technological parameters for automatic submerged-arc cladding by strips were the following, namely I_w = 650 A, voltage U_a = 32 V, width of strip electrode 60 mm, temperature of preheating and concurrent heating T_h = 250 °C, cladding rate v_c = 10 m/h.

Technological parameters for manual arc cladding with coated electrodes are the next [29], namely current intensity I_w = 130–150 A, U_a = 26–30 V, electrodes of 4–5 mm diameter, temperature of preliminary and concurrent heating T_h = 250 °C, cladding rate v_s = 3 m/h.

Composition of base material of steel 15Kh2NMFA RV is presented in Table 3 [30]. Thermal-physical properties of base metal and RV cladding consumable depending on temperature are given in works [31, 32].

Experimental procedure. Physical modeling on Gleeble 3800 unit using cylindrical samples of steel 15Kh2NMFA of 6 mm diameter and 76 mm length were used to get experimental results of microstructure composition of HAZ metal after arc cladding. CCT diagrams of austenite decay at cooling rates 1, 3, 5, 7 °C/s were plotted.

Metallographic examinations were carried out after modeling of structural transformations in the samples. The samples were chemically etched in 4 % alcoholic solution of nitric acid (nital) for microstructure detection. Examination of microstructures was carried out on NEOPHOT-32 microscope equipped with digital add-on device OLYMPUS at ×200 and ×500 magnifications. Vickers hardness measurement was performed on hardness gauge M-400 of LECO Company at 100 g and 1 kg loading. Composition of 15Kh2NMFA steel samples (Table 3) was determined on atomic emission spectrometer with inductively-coupled plasma ICAP 6500 DUO (TERMO FISHER SCIENTIFIC, USA). Content of carbon was determined by coulometric method. According to [3–5] the parts of RV from 15Kh2NMFA steel in initial state have bainite structure (V_b = 1.0).

Mathematical model. Mathematical modeling was carried out on a model of nozzle zone of WWER-

Table 2. Consumables for anti-corrosion cladding

Surface type	Double-layer cladding	Grade of consumables	Flux
Cylindrical surface of vessel	First layer	Sv-07Kh25N13, TU 14—1-3146–81	48-OF-10, OST 5.9206–75
	Second layer	Sv-04Kh10N19G2B, TU 141-14591–89	FTs-18, OST 24.948.02–99
Inner surface of nozzles	First layer	TsL-25/1, ZIO-8, GOST 9466–75	–
	Second layer	EA-898/21B, TsT-15K, GOST 10052–75	–

Table 3. Composition of examined steel 15Kh2NMFA, wt.%

Sample	C	Si	Mn	Cr	Ni	Mo	Cu	V	S	P
	0.17	0.28	0.41	2.04	1.37	0.63	0.03	0.12	0.01	0.01
Standard TU 108-765–78	0.13–0.18	0.17–0.37	0.3–0.6	1.8–2.3	1.0–1.5	0.5–0.7	≤0.3	0.10–0.12	≤0.02	≤0.02
Note. Base — iron. Content of elements shall not exceed, wt.%: Co ≤ 0.03 %; As ≤ 0.04 %. For steel 15Kh2NMFA-A content of elements shall not exceed, wt.%: %: Sn ≤ 0.005; Sb ≤ 0.005; Cu ≤ 0.10; S ≤ 0.012; P ≤ 0.010; As ≤ 0.010.										

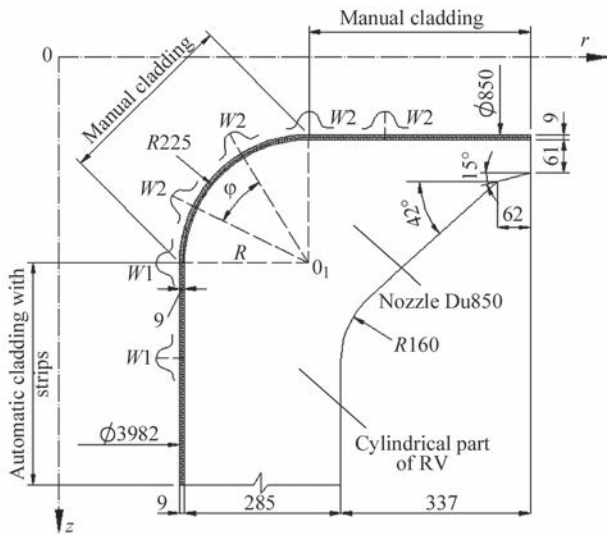

Figure 1. Scheme of nozzle zone of RV and location of areas with different technologies of arc cladding

1000 RV, cladding of which is performed on both mentioned above technologies (Figure 1). In a calculation finite-element model of the nozzle zone there were used two types of sources of cladding heating (strip — for vessel shell and spot, simulating manual cladding with coated electrodes, for inner surface of Du850 nozzle as well as fillets). A temperature problem was solved in 2D problem formulation at assumption of fast moving heat source and axial symmetry of cladding of protective layers at boundary condition of convective heat exchange with environment. Distribution of heat power of strip source W_1 and spot source W_2 with 2D formulation in a cylindrical coordinate system can be described by dependencies (1) and (2), respectively:

$$W_1(r, z, t) = \frac{2Q\sqrt{K_r K_z}}{\pi v t_h \left[1+\sqrt{\frac{K_z}{\delta}}b\right]} \times \times \exp\left[-K_r D_r^2 - K_z D_z^2\right]; \quad (1)$$

$$W_2(r, z, t) = \frac{2Q\sqrt{K_r K_z}}{\delta v t_h} \exp\left[-K_r D_r^2 - K_z D_z^2\right], \quad (2)$$

where $D_z = z - z_0$; $D_r = r - r_0$; r, z are the coordinates (radial and axial) of considered point of the nozzle zone; r_0, z_0 are the coordinates of a center of moving heat source; K_r; K_z are the coefficients of concentration of specific heat flow; t_h is the heating time; Q is the effective power of heating source ($Q = \eta I_w U_a$); η is the efficiency coefficient; v is the cladding rate; b is the strip width.

Distribution of residual stresses in vessel material depends on microstructure composition and, respectively, mechanical properties in MZ and HAZ. In accordance with calculation approach [18, 19], based on application of parametric regression equations, the results of calculation of weight fraction of each microstructure phase (V_m — martensite; V_b — bainite; V_{fp} — ferrite-pearlite) in a final structure after cooling depend on composition of steel and typical time $\Delta t_{8/5}$ (s) of cooling from 800 to 500 °C temperature.

$$\text{Martensite } V_m^{max} = 0.5\left[1 - erf\,\frac{\ln \Delta t_{8/5} - \ln \Delta t_m^{50}}{\ln S_m}\right]; \quad (3)$$

$$\text{Ferrite-pearlite } V_{fp}^{max} = 0.5\left[1 + erf\,\frac{\ln \Delta t_{8/5} - \ln \Delta t_{fp}^{50}}{\ln S_{fp}}\right]; \quad (4)$$

$$\text{Bainite } V_b^{max} = 1 - V_m^{max} - V_{fp}^{max}, \quad (5)$$

where Δt_m^{50} is the time (s) of cooling from 800 to 500 °C temperature, at which in microstructure after cooling there is formation of 50 % of martensite ($V_m^{max} = 0.5$); $^{50}_{fp}$ is the time (s) of cooling from 800 °C to 500 °C temperature, at which in microstructure after cooling there is formation of 50 % of ferrite-pearlite ($V_{fp}^{max} = 0.5$); S_m, S_{fp} are the parameters of model of austenite decay.

Values of parameters Δt_m^{50}, Δt_{fp}^{50}, S_m, S_{fp} for low-alloy steels (weight fraction %: $0.05 \le C \le 0.4$; $Mn \le 2$; $Si \le 0.8$; $Cr \le 2$; $Mo \le 1$; $Ni \le 1.5$; $V \le 0.2$; $Ti \le 0.03$; $Al \le 0.05$; $Nb \le 0.03$) are determined according to data of work [18] depending on steel composition.

Results of mathematical modeling. Solution of a nonstationary heat conduction problem provided the calculation data of fields of the maximum temperatures and typical thermal cycles in cladding, which allowed evaluating the dimensions of HAZ and cooling rates of metal of the nozzle zone at different technological parameters (Figure 2, Table 4).

Obtained modeling results for two technologies of arc cladding showed (Figure 3) that automatic cladding in HAZ metal provokes formation of bainite-martensite structure, martensite fraction makes up to 12 %. Fraction of martensite in HAZ metal reaches 48 % in manual arc cladding with coated electrodes due to higher cooling rate.

Obtained calculation results relatively to bainite-martensite microstructure of 15Kh2NMFA steel after cladding have sufficiently good agreement with the reference data [11].

To check the obtained calculation data the experiments on physical modeling of thermal cycles

Table 4. Results of calculation of HAZ size and cooling rates for different technological parameters of cladding

Technology of arc cladding	Width of bead, mm	Temperature of preheating, °C	HAZ size, mm	Cooling rate $w_{8/5}$, °C/s
Manual with coated electrodes	15	250	6	8–9
Automatic submerged-arc	60	250	10	4–5

of cladding of samples from steel 15Kh2NMFA using Gleeble 3800 were carried out and examination of their microstructure was performed. Gleeble 3800 modeling provided research of several modes simulating thermal cycles of cladding, namely at constant cooling rates, with cooling on real thermal cycle of cladding, with holding and without holding at maximum temperature of thermal cycle, at different maximum temperature of welding cycle.

Physical modeling of thermal cycle with long-term holding at heating. Examined sample was heated to 1000 °C per 10 min, was hold at 1000 °C temperature for 170 min, that made the total time of heating 180 min, with next cooling at constant rate 1; 3; 5; 7 °C/s. Record of dilatometric data took place in process of thermal effect. They were used for plotting CCT diagram of undercooled austenite decay. To evaluate reliability of obtained results the experimental CCT diagram was compared with existing CCT diagram for steel 15Kh2NMFA [15] (Figure 4).

Analysis of obtained CCT diagram of steel 15Kh2NMFA showed that it considerably different from existing one. The differences lie in presence of a high-temperature field of bainite transformation within the limits of all investigated rates of cooling. Whereas, in the austenite decay diagram [15] bainite transformation finishes at 5 °C/s cooling rate. The temperatures of start of bainite transformation in the

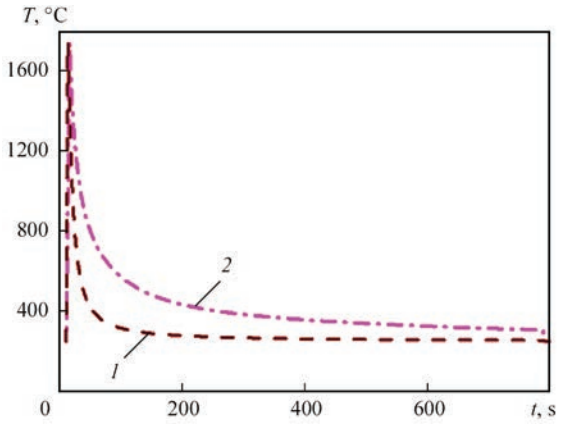

Figure 2. Typical thermal cycles in manual arc cladding with coated electrodes (*1*) and automatic submerged-arc cladding with 60 mm strip (*2*)

existing CCT diagram reach 550–560 °C for low cooling rates, whereas in the experimental diagram the temperature of start of bainite transformation reaches 607 °C for cooling rate 1 °C/s (Table 5).

Temperature of start of martensite transformation in the examined samples is sufficiently close to the reference data. The results of metallographic examinations of the samples at cooling rates 1, 3, 5, 7 °C/s are presented in Figure 5.

Fraction of structural constituents in the examined samples was determined using the methods of quantitative metallography (Table 6).

The analysis of obtained data showed that rise of cooling rate provokes increase of martensite fraction from 8 to 80 % (based on the results of structural analysis) or from 26 to 66 % (based on Gleeble results), and hardness of microstructure HV1 rises from 3530–3780 MPa to 4700–4820 MPa.

Physical modeling of thermal cycle without long-term holding at heating. Additional modeling was carried out at cooling rate 5 °C/s , however, without long-term holding and at accelerated heat-

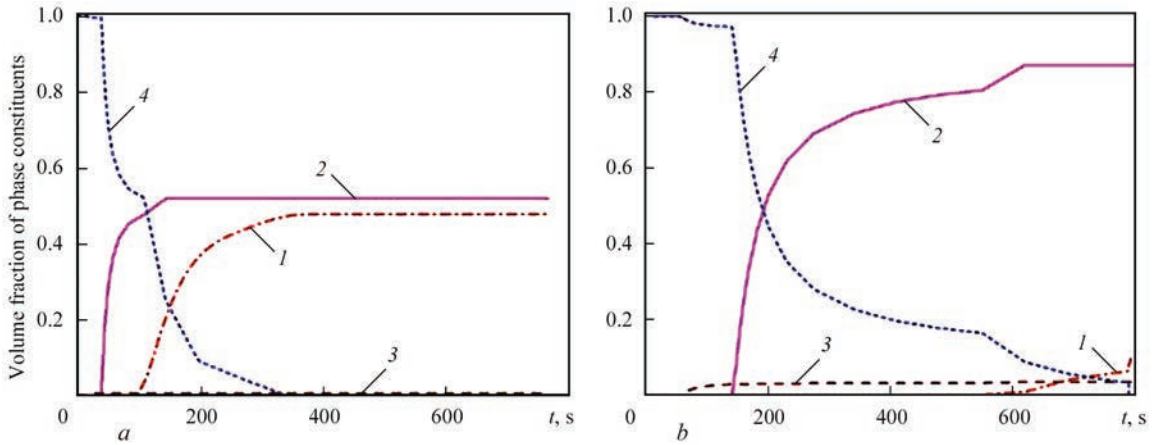

Figure 3. Results of calculation prediction of austenite decay kinetics in HAZ metal in arc cladding: *a* — manual arc cladding with coated electrodes; *b* — automatic submerged-arc cladding with strip *b* = 60 mm (*1* — martensite; *2* — bainite; *3* — ferrite-pearlite; *4* — austenite)

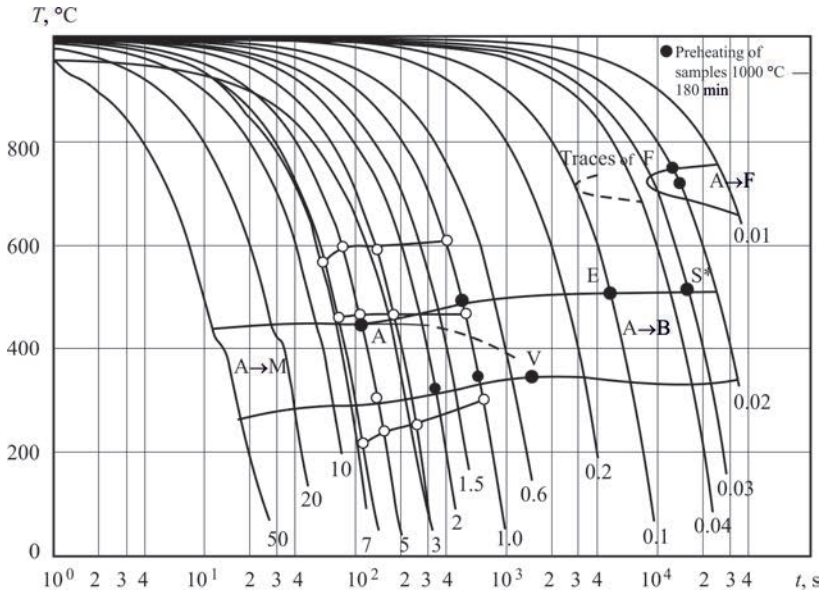

Figure 4. Comparison of obtained experimental (○) and existing (●) [15] CCT diagram of austenite decay of steel 15Kh2NMFA

Table 5. Temperatures of bainite and martensite transformation of steel 15Kh2NMFA

Cooling rate $w_{8/5}$, °C/s	Temperature of start of bainite transformation, °C	Temperature of bainite-martensite transformation, °C	Temperature of end of martensite transformation, °C	A_{c1}, °C	A_{c3}, °C
1	607	464	302	683	858
3	590	465	253	672	861
5	600	464	243	704	861
7	568	460	215	690	866

ing in order to reduce metal staying in a high-temperature state. The proposed thermal mode included heating to 1000 °C, holding at this temperature during 1 s and further cooling at constant rate 5 °C/s. The temperature mode being modeled has more reliable correspondence to real heating/cooling conditions of HAZ metal in arc welding/cladding of 15Kh2NMFA steel. The analysis showed sufficiently good correspondence of experimental data and data of work [15] on temperature transformations in steel 15Kh2NMFA at thermal cycle without long-term holding with constant cooling rate 5 °C/s. Thus, temperature of start of martensite transformation 452 °C well matches to similar temperature on CCT diagram, presented in work [15], which makes 445 °C. Temperature of end of martensite transformation 320 °C also almost matches with the temperature of martensite transformation end 300 °C at given cooling rate. The results of quantitative analysis of microstructure verified formation of almost completely 100 % martensite structure. Experimentally observed presence of an inflection on the transformation curve at 200 °C, apparently, related with «rigid» nature of sample fixing in modeling.

Table 6. Results of metallographic analysis

Cooling rate $w_{8/5}$, °C/s	Vickers hardness *HV*1, MPa	Fraction of bainite/martensite on results of structure analysis, %	Fraction of bainite/martensite on Gleeble results, %
1	353–378	92/8	74/26
3	407–467	37/63	44/55
5	439–476	32/68	41/59
7	470–482	20/80	34/66

Physical modeling of real welding thermal cycle. In real technological process of welding/cladding, metal cooling does not take place on a linear dependence, however, such approach allows significantly simplifying the process of physical modeling. The real cladding thermal cycle was programmed in the work. It corresponded to cooling from 1000 °C with 5 °C/s rate in 800–500 °C temperature range.

Figure 6 shows a comparison of obtained data of real cooling cycle with cooling cycle at constant rate without long-term holding. Analysis of the transformation curves allowed determining the temperatures of transformation start, formation of intermediate (martensite) phase and temperature of transformation end (Table 7).

Figure 7 presents the comparison of dilatometric curves at different cooling cycles. Analysis of the dilatograms shows that transformation start for both thermal cycles takes place at temperature close

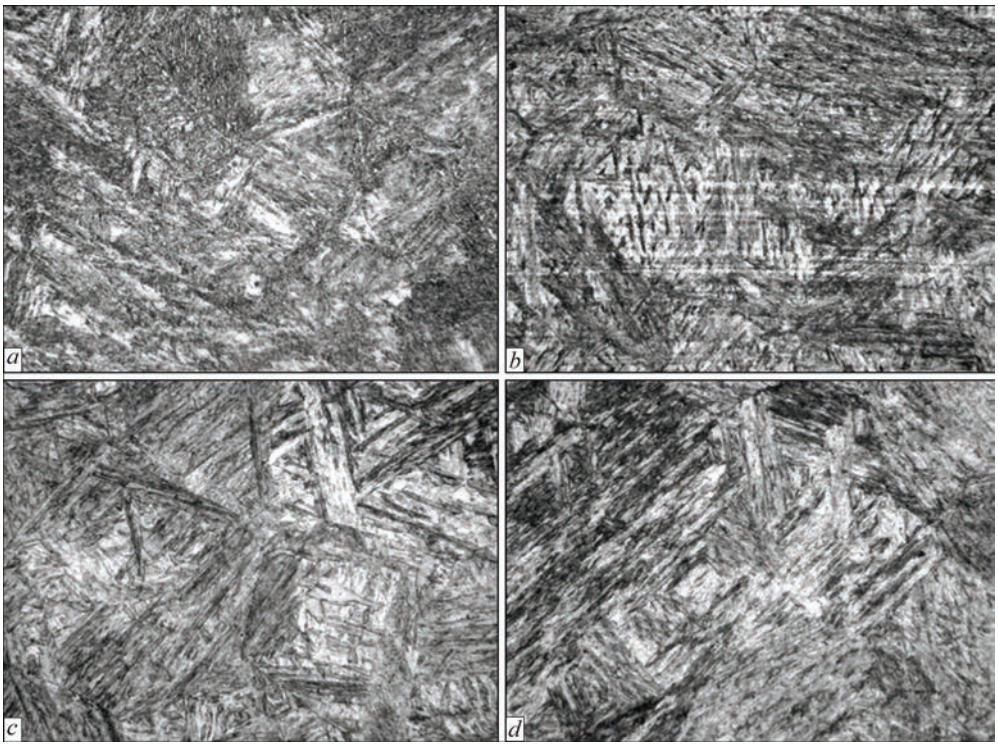

Figure 5. Microstructure (×500) of samples of steel 15Kh2NMFA after holding at 1000 °C temperature during 170 min and further cooling at rates: *a* — 1; *b* — 3; *c* — 5; *d* — 7 °C/s

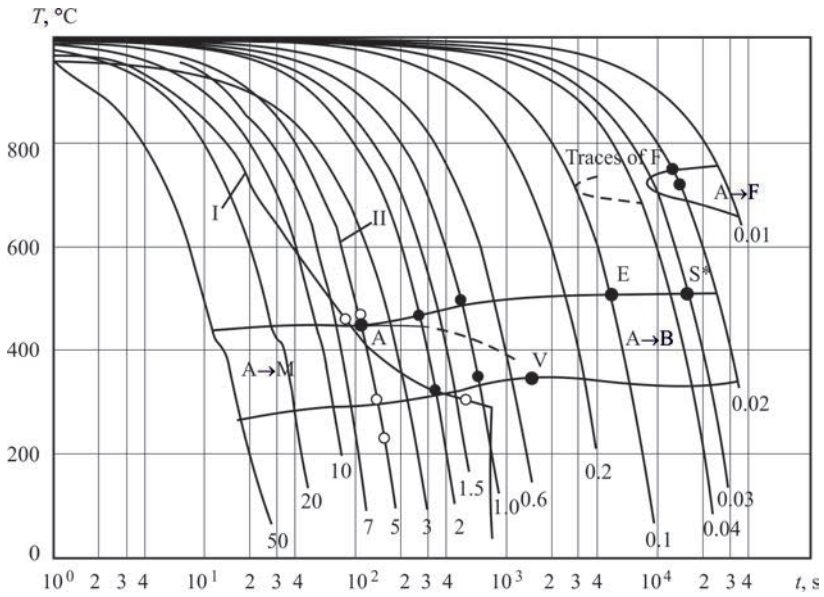

Figure 6. Comparison of data of transformation CCT diagram obtained at cooling of sample on real welding thermal cycle (I) and on thermal cycle with constant cooling rate (II) [15]

Table 7. Temperatures of bainite and martensite transformations of steel 15Kh2NMFA under conditions of thermal welding cycle

Modeling conditions	Temperature of transformation start, °C	Temperature of intermediate phase, °C	Temperature of transformation end, °C	A_{c1}, °C	A_{c3}, °C
Without long-term holding, at constant cooling rate	466	306	231	683	858
Real thermal cycle	460	–	304	672	861

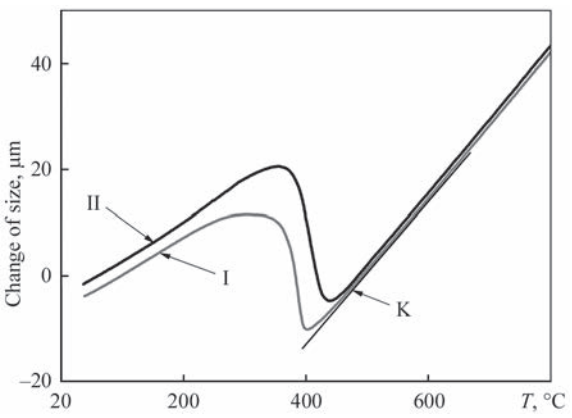

Figure 7. Dilatograms of transformations obtained at constant cooling rate (I) and at cooling on real thermal cycle of cladding (II); K — area of transformation start, deviation of both dilatograms from area of linear thermal expansion

to 460–466 °C, and conditional transformation rate (change of fraction of phase depending on temperature) in the field of developed transformation (middle part) is also virtually similar (angle of curves' inclination). Significant differences in the transformation nature are observed in the field of martensite formation (250–350 °C), where curves' nature is different.

Obtained data of dilatometric investigation allow making a conclusion that morphology of microcrystalline structure of the sample after thermal cycle at constant cooling rate and sample after real thermal cycle has small differences.

Figure 8 presents the comparison of microstructures of the samples, obtained at constant cooling rate without long-term holding and on real welding cycle.

Structure of the samples, obtained at constant cooling rate 5 °C/s without long-term holding in austenite area presents itself the structure of fine acicular martensite (Figure 8, *a*). The sample can contain small amount of bainite up to 3–5 %. Vickers hardness HV1 of this structure changes from 4460 to 4580MPa.

Structure of the sample, obtained on real welding cycle, is extremely inhomogeneous and presents itself banded structure consisting of alternating longitudinal areas of dispersed and coarse acicular structure (Figure 8, *b*). The areas of dispersed structure present themselves the areas of fine acicular martensite, and coarse acicular ones are the areas of lower bainite. Vickers hardness *HV*1 of the given structure changes from 3940 to 4460 MPa. The results of quantitative metallography show that the fraction of structures in the examined samples made 80–90 % of martensite and 10–20 % of bainite.

Thus, comparison of microstructures of examined samples shows that regardless the fact that an average cooling rate in both samples in transformation area 800–500 °C was almost similar and made 5 °C/s, the structures forming in the process of 15Kh2NMFA steel cooling somewhat differ from each other. In the one case, there is formation of completely martensite structure, whereas in the another it is martensite-bainite.

Metallographic examinations of samples of 15Kh2NMFA steel at different maximum temperatures of welding cycle. Metallographic examinations of the samples after simulation of real welding thermal cycles on Gleeble 3800 differing by maximum heating temperature are presented in Figure 9.

Structure of the sample, obtained on real welding thermal cycle at maximum heating temperature 1000°C is characterized with banded inhomogeneous structure consisting of alternating bands of dispersed fine acicular martensite (80–90 %) and coarse acicular structure of lower bainite (10–20 %) (Figures 8, *b*, 9, *a*).

Structure of the sample, obtained on real welding thermal cycle at maximum heating temperature 1350 °C is characterized by homogeneous martensite structure (Figure 9, *b*). Size of the coarse martensite packages made 50–60 μm fine — 20–30 μm. Size of the martensite grains corresponds to 3.5–4 grain size number on ASTM (100–120 μm). Vickers hardness *HV*1 of given structure changes from 4130 to 4530 MPa. The fraction of structures in the examined sample based on the results of quantitative metallography made 100 % of martensite.

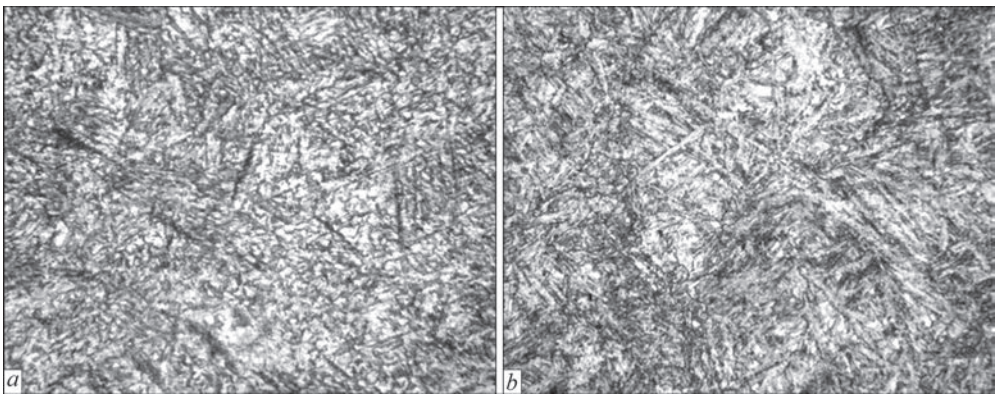

Figure 8. Microstructure (×500) of sample at 5 °C/s without long-term holding with constant cooling rate (*a*) and obtained on real welding cycle (*b*)

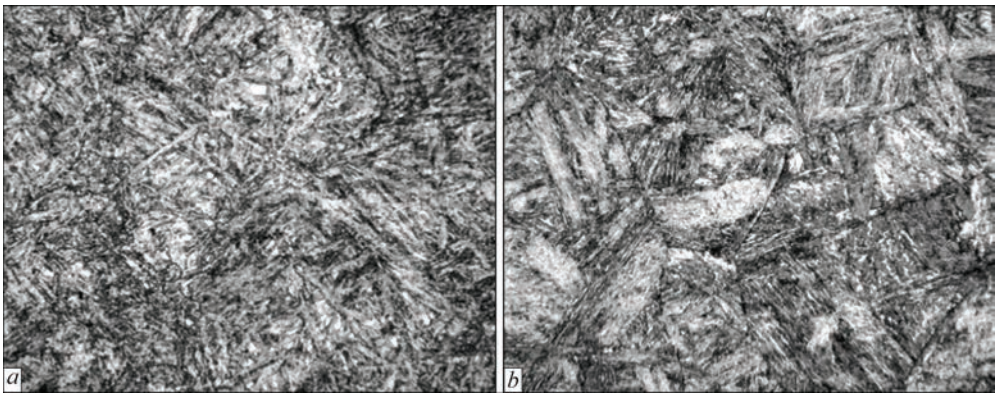

Figure 9. Microstrucutre (×500) of sample at 5 °C/s obtained on real thermal cycle at maximum heating temperature 1000 (*a*) and 1350 °C (*b*)

Thus, comparison of microstructures of the examined samples shows that increase of the maximum heating temperature from 1000 to 1350 °C results in significant growth of primary austenite grain, completely eliminates banded orientation of the structure, caused by machining (rolling) of initial sheets of steel 15Kh2NMFA, and leads to formation of completely martensite structure with higher level of hardness in contrast to martensite-bainite structure, forming in the sample at maximum temperature cycle 1000 °C.

Comparison of the dilatometric curves of real welding cycle, obtained at different maximum temperatures of the cycle without holding, is shown in Figure 10.

The analysis of obtained results showed that the transformation curves have various nature. On heating stage to 900 °C temperature the dilatometric curves completely correspond each other. At maximum heating temperature 1350 °C the transformation in high-frequency area starts at 1050 °C temperature and ends at 1250 °C temperature, that corresponds to formation in this area of δ-ferrite structure. In modeling of the cycle with maximum heating temperature 1000 °C, it becomes apparent that formation of δ-ferrite is absent due to insufficient heating temperature.

Investigation of transformation kinetics showed that the transformation takes place on a compatible mechanism and has similar nature. The difference in kinetic transformation curves for the maximum heating temperatures makes 10–15 °C (Figure 11).

The analysis of obtained dilatometric results allows making a conclusion that change of the maximum temperature of heating almost has no effect on kinetics of formation of martensite phase, inconsiderably influences the temperatures of start and end of phase formation, but has obvious effect on total value of martensite transformation (dilatometric effect).

Plotting the CCT diagrams of austenite decay for two maximum temperatures of welding thermal cycle. Based on carried thermal deformation investigation using Gleeble 3800 unit and further metallographic analysis of the samples for typical thermal cycles of welding/cladding at different rate of cooling in 800–500 °C range and two different maximum temperatures of heating there were obtained two welding CCT diagrams for steel 15Kh2NMFA (Figure 12).

Comparison of experimental CCT diagrams with existing one [15] indicates small difference in the values of temperatures of start and end of transformations (in 50 °C limits) as well as the main difference — range of martensite-bainite transformation

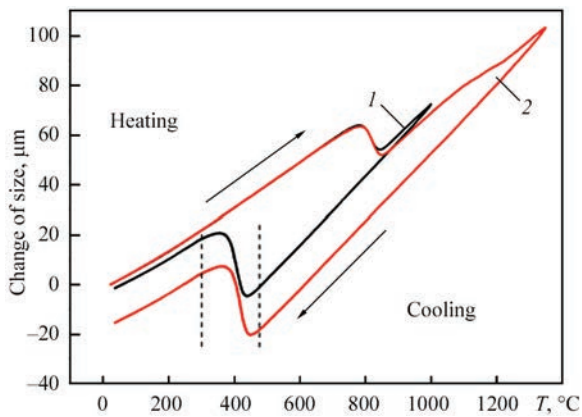

Figure 10. Dilatograms of transformations obtained at different maximum temperatures of thermal cycle: *1* — 1000; *2* — 1350 °C

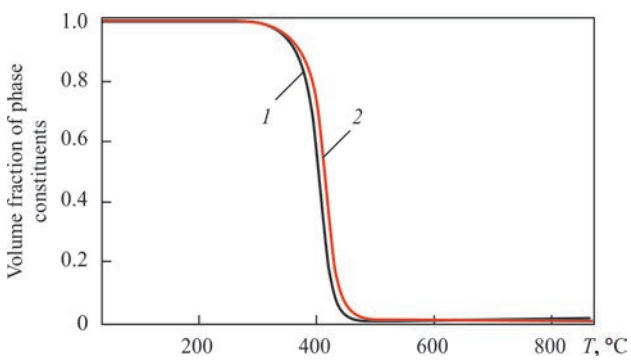

Figure 11. Dependence of fraction of forming phase on temperature for real thermal cycle depending on maximum temperature of heating: *1* — maximum heating temperature 1000; *2* — 1350 °C

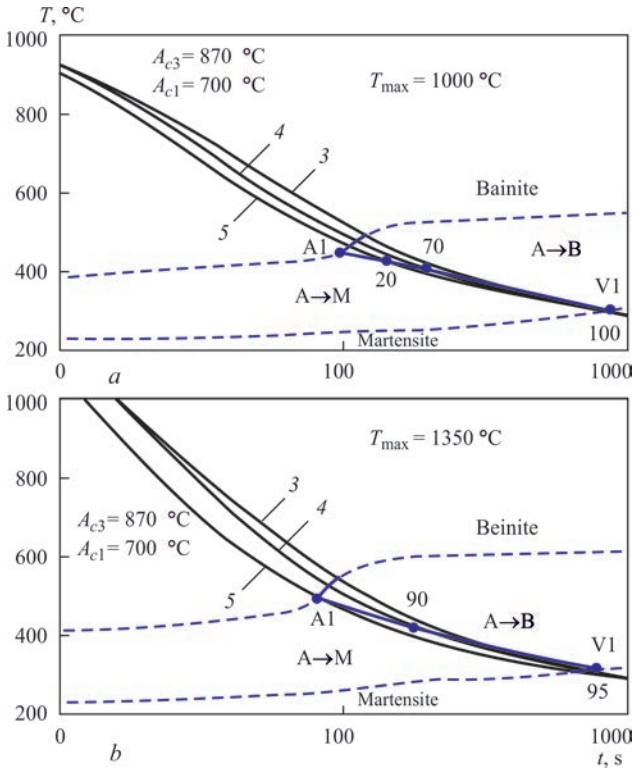

Figure 12. CCT diagrams of austenite decay for steel 15Kh2NMFA for typical welding cycles of cooling at maximum heating temperature: *a* — 1000; *b* — 1350 °C (*3–5* — cooling rate) in 800–500 °C range

and its critical cooling rate. Following existing diagram point *A* corresponds to start of range of martensite – bainite transformation (100 % of martensite, cooling rate 5 °C/s), point *B* — end (100 % of bainite, 0.6 °C/s). This is so called critical cooling rates in the range of martensite and bainite transformations.

According to the experimental diagrams in Figure 12 the points of start and end of range of martensite-bainite transformation correspond to the points *A*1 and B1, which do not match with points *A* and *B* of existing diagram in Figures 4, 6. Point *A*1 (critical point of martensite transformation) lies on the cooling curve 5 °C/s, the same as point *A* and point *B*1 (critical point of bainite transformation) on cooling curve 3 °C/s that do not correspond point *B* (0.6 ≈ °C/s) of the diagram from work [15].

It can be concluded that following the experimental data obtained for real welding thermal cycles, range of cooling rates of martensite-bainite transformation is narrower than in the existing CCT diagrams of austenite decay [8, 15, 16] obtained at long-term holding at the stage of heating and further constant cooling rate.

Conclusions

1. The comparative analysis of calculation results showed significant effect of technological parameters of the process of arc cladding on the kinetics of microstructure transformations and residual microstructure-phase composition in HAZ metal of vessel steel 15Kh2NMFA. Application of the procedure based on parametric regression equations allows calculation of structure phase composition of HAZ metal: for a mode of manual arc cladding with coated electrodes ($w_{8/5}$ = 8–9 °C/s) the maximum content of martensite is around 50 %, for automatic submerged-arc cladding with strip electrodes ($w_{8/5}$ = 4–5 °C/s) the maximum content of martensite does not exceed 15 %.

2. Experimentally determined that in the researched range of cooling rates 1–7 °C/s the final microstructure of HAZ metal of steel 15Kh2NMFA at long-term holding 180 min at 1000 °C temperature in austenite area consists of bainite-martensite mixture, and at short-term holding 1 s from martensite. It can be concluded that long-term holding at 1000 °C temperature, designed for complete austenitizing of metal before cooling on welding thermal cycle is not adequate condition for reliable physical modeling.

3. Comparison of CCT diagram of the samples obtained at cooling with constant rate and on real welding cycle showed that kinetics of transformation at constant cooling rate takes place at lower by 20–30 °C temperatures in comparison with the transformation on real welding cycle. The structure of sample obtained at constant cooling rate 5 °C/s without long-term holding in austenite area presents itself a structure of fine acicular martensite, whereas the sample structure obtained on real cooling cycle of welding (average rate 5 °C/s), consists of areas of fine acicular martensite and lower bainite to 10–20 %.

4. It was shown how the maximum temperature of heating 1000 and 1350 °C effects the nature of transformation, microstructure, fraction of forming phases, position of temperatures of start and end of bainite and martensite transformation.

5. Comparison of obtained experimental data and results of mathematical modeling of microstructure transformations at real cooling cycle of cladding verify formation of bainite-martensite structure in HAZ metal of WWER-1000 RV, however the value of martensite content significantly differs (the difference makes up to 50 %). For calculation determination of content of structure-phase constituents it is necessary to use the experimental data of CCT diagram of undercooled austenite decay for typical welding/cladding thermal cycles, in which long-term heating (holding) at austenitizing temperature is absent and cooling takes place with variable rate.

6. For adequate evaluation of microstructure phase composition in HAZ metal of vessel steel 15Kh2NMFA in welding/cladding there were plotted CCT diagrams of undercooled austenite decay for

typical cooling rates 3–5 °C and two maximum temperatures of thermal cycle 1000 and 1350 °C.

Obtained investigation results can be used for calculation determination of residual stresses in WWER-1000 RV at justification of extension of safe operation life.

1. (1989) PNAE G-7-002-86: *Codes of design on strength of equipment and pipings of nuclear power plants*. Gosatomenergonadzor SSSR. Moscow, Energoatomizdat [in Russian].
2. Khlybov, A.A., Uglov, A.L. (1998) Determination of physico-mechanical characteristics of material of specimens subjected to radiation. *Trudy NizhGTU*, **1**, 220-228 [in Russian].
3. Gurovich, B.A., Kuleshova, E.A., Fedotova, S.V. (2011) *Influence of chemical composition and structural parameters of steels of WWER reactor vessels on susceptibility to embrittlement caused by formation of grain-boundary segregations, including under conditions typical for long-term operation of power plants*. Moscow, NRC Kurchatov Institute [in Russian].
4. Frolov, A.S. (2013) *Phase-structural state and operating characteristics of new compositions of steels for reactor vessels with higher power and service life*: Syn. of Thesis for Cand. of Techn. Sci. Degree. Moscow, NRC Kurchatov Institute [in Russian].
5. Markov, S.I. (2012) *Metal science principles of manufacture of billets for high-reliability elements of power and piping systems*: Syn. of Thesis for Dr. of Techn. Sci. Degree. Moscow, TsNIITMASh [in Russian].
6. Margolin, B.Z., Shvetsova, V.A., Gulenko, A.G. et al. (2002) Prediction of crack resistance of vessel reactor steel based on concept of «Mastercurve» and probabilistic model. *Problemy Prochnosti*, **1**, 5–21 [in Russian].
7. Fomenko, V.N. (2017) *Prediction of fracture toughness for calculation of strength of WWER type reactor vessels on the base of witness-specimen tests and local criteria of brittle fracture*: Syn. of Thesis for Cand. of Techn. Sci. Degree. Saint-Petersburg, CRI CM «Prometheus» [in Russian].
8. Popova, L.E., Popov, A.A. (1991) *Transformation diagrams of austenite in steels and beta solution in titanium alloy*: Refer. Book of heat-treater. 3rd Ed., Moscow, Metallurgiya [in Russian].
9. Karzov, G.P., Margolin, B.Z., Teplukhina, I.V., Piminov, V.A. (2016) *Materials science aspects of increase of operation safety of WWER type power plants on the base of reactor vessel steel improvement*. Saint-Petersburg, CRI CM «Prometheus», Podolsk, OKB Gidropress JSC [in Russian].
10. Livshits, L.S., Khakimov, A.N. (1989) *Physical metallurgy of welding and heat treatment of welded joints*. 2nd Ed., Moscow, Mashinostroenie [in Russian].
11. Margolin, B.Z., Varovin, A.Ya., Kostylyov, V.I. (2005) Determination of residual stresses in the WWER vessels after multirun welding, surfacing and high-temperature tempering. *The Paton Welding J*., **10**, 14–20.
12. (1977) *Atlas of isothermal transformation and cooling transformation diagrams. American Society for Metals*.
13. *Zhang* Zhuyao, Farrar, R.A. (1995) *An atlas of continuous cooling transformation diagrams (CCT) applicable to low carbon low alloy weld metals*. London, Institute of Materials.
14. Zeyffarth, P. (1982) *Atlas Schweiss-ZTU-Schaubilder*. Berlin, VEB Verlag Technik, Duessseldorf, DVS-Verlag.
15. *Center of modeling of casting processes and technologies*. http://mip-cast.ru/treatment
16. Teplukhina, I.V., Golod, V.M., Tsvetkov, A.S. (2018) CCT diagram plotting based on the numerical analysis of dilatometric tests results. *Letters on Materials*, 8(**1**), 37–41.
17. Soloviov, I.V., Kornienko, O.Yu, Zhilyakov, A.Yu., Belorusets, A.M. (2017) Investigation of decay kinetics of overcooled austenite of steel 15Kh2NMFA during continuous cooling. In: *Proc. of 18th Int. Sci.-Techn. Conf. of Ural School-Seminar of Metallurgists-Young Scientists (Russia, Ekaterinburg, 21-23 November 2017)*. UrFU, 250–252.
18. Kasatkin, O.G., Zeyffarth, P. (2002) Calculated models for evaluation of mechanical properties of HAZ metal in welding of low-alloy steels. In: *Proc. of Int. Conf. on Mathematical Modeling and Information Technologies in Welding and Related Processes*. Kiev.
19. Makhnenko, V.I., Velikoivanenko, E.A., Pochinok, V.E. et al.(1999) Numerical methods for the prediction of welding stress and distortions. *Welding and Surfacing Reviews*, **13**, Pt 1, 1–146.
20. *Dean* Deng, Yangang Tong, Ninshu Ma, Hidekazu Murakawa (2013) Prediction of the residual welding stress in 2.25 Cr–1Mo steel by taking into account the effect of the solid-state phase transformations. *Acta Metall. Sin*., 26(**3**), 333–339.
21. *Yukio* Ueda, Hidekazu Murakawa, Yu Luo (1995) A computational model of phase transformation for welding processes. *Transact. of JWRI*, 24(**1**), 95–100.
22. (2003) PNAE G-7-009–89: *Equipment and pipings of nuclear power plants*. Welding and surfacing, fundamentals. Moscow [in Russian].
23. *ZhNPP-1 reactor vessel. 1152.02.70.000. Certificate of pressure vessel* [in Russian].
24. Dub, A.V. (2013) *Development of main structural materials for WWER reactors, SRTs RF*. Podolsk, NPO TsNIITMASh [in Russian].
25. Voronov, A.V. (2013) *Improvement of quality of welded joints and deposited surfaces of NPP equipment*. Saint-Petersburg, PJSC «Izhora Plants» [in Russian].
26. *Iradj* Sattari-Far, Magnus Andersson (2006) Cladding effects on structural integrity of nuclear components. SKI Report 2006:23, ISSN 1104-1374, ISRN SKI-R-06/23-SE.
27. Katsuyama, J., Udagawa, M., Nishikawa, H. et al. (2010) Evaluation of weld residual stress near the cladding and J-weld in reactor pressure vessel head for the assessment of PWSCC behavior. *E-J. of Advanced Maintenance, **2**, Japan Society of Maintenology*, 50–64.
28. Dupas, P., Moinereau, D. (1996) Evaluation of cladding residual stresses in clad blocks by measurements and numerical simulations. *J. de Physique IV Colloque*, **06**(C1), 187–196.
29. Tsvitanovich, M., Postruzin, Zh., Munk, R. et al. (2011) Systems of ultrasonic testing of metal of NPP reactor vessel Kudankulam. In: *Proc. of Conf. on Safety Assurance of NPP with WWER, Podolsk, OKB Gidropress* [in Russian].
30. *TU 108-765–78:* Billets from steel of 15Kh2NMFA and 15KhNMFA-A grades for vessels and covers and other assemblies of reactor plants.
31. Kostylev, V.I., Margolin, B.Z. (2000) Determination of residual stress and strain fields caused by cladding and tempering of reactor pressure vessels. *Int. J. of Pressure Vessels and Piping*, **77**.
32. (2000) *Procedure for determination of service life of nuclear reactor vessels during operation (MRK-SKhR-2000), RD EO 0353-02*, Saint-Petersburg-Moscow [in Russian].

Received 21.05.2019